Towards the optimization of a simple route for the fabrication of energy-efficient VO_2-based smart coatings

Antonio Jesús Santos[a,b,c,*], Nicolas Martin[c], Javier Outón[a,d], Eduardo Blanco[a,d], Rafael García[a,b], and Francisco Miguel Morales[a,b]

[a] *IMEYMAT: Institute of Research on Electron Microscopy and Materials of the University of Cádiz, Spain.*

[b] *Department of Materials Science and Metallurgic Engineering, and Inorganic Chemistry, Faculty of Sciences, University of Cádiz, Spain.*

[c] *Institut FEMTO-ST, UMR 6174 CNRS, Université Bourgogne Franche-Comté, 15B, Avenue des montboucons 25030 Besançon Cedex, France.*

[d] *Department of Condensed Matter Physics, Faculty of Sciences, University of Cádiz, 11510 Puerto Real, Cádiz, Spain.*

* Corresponding author: antonio.santos@uca.es

Abstract: The present work reports on the optimization of a simple two-step procedure to achieve thermochromic vanadium dioxide coatings. The effect of the layer thickness, the total surface area exposed, as well as different parameters involved in a fast annealing process leads to the selective oxidation in air atmosphere of vanadium films sputtered at glancing angles. Outcomes resulting from structural and optical characterizations of annealed films with different layer thicknesses and porosities disclose two optimal pathways for the fast heating synthesis of high-performance VO_2-based coatings with unique thermochromic features. A first one at 475ºC with reaction times ranging from 40–60 s, ideal for thicker films (~100 nm), which implies reaching pseudo-equilibrium states with the formation of a VO_2 + VO_{2+x} phase mixture. A

second one more adapted for thinner samples (~25 nm), which involves obtaining VO_2-refined products through instantaneous reactions at 500ºC. The unusual balance achieved for luminous transmittance (> 60%) and solar modulation ability (~5%) through the second route, coupled with a remarkable decrease in the metal-to-insulator transition temperature without the need of using doping (up to 15°C below that of the pure bulk VO_2, i.e., ~68°C), make these initially porous systems potentially applicable in energy efficient smart glazing or resistive switching while paving the way for further initiatives towards the simple and cost-effective manufacturing of VO_2 thermochromic coatings at a large scale.

Keywords: Vanadium dioxide, thin film, glancing angle deposition, rapid thermal annealing, Vis-NIR spectrophotometry, metal-insulator transition, smart window.

1. Introduction

Vanadium dioxide (VO_2) is a thermochromic material that has attracted extensive attention from scientists and technologists because of its unique metal-insulator transition (MIT) at near room temperature[1,2]. This phenomenon not only leads to structural changes between monoclinic VO_2(M1) to rutile VO_2(R), but also to strong alterations in electrical resistivity and infrared transmission over the MIT. This makes it a suitable material for applications such as electrical switches[3,4], memory devices[5], or smart radiators[6], among others. In this same vein, VO_2-based thermochromic coatings with a self-blocked infrared transmittance above a critical MIT temperature (T_c) can also be used to regulate the transmittance of solar heat (T_{sol}) in energy-efficient smart windows[7–13]. Current requirements for the application of these smart coatings in building glazing imply luminous transmittances (T_{lum}) greater than 60% (for the maximum use of sunlight), solar modulation abilities (ΔT_{sol}) over 10% (for efficient adaptation to climate changes), and MIT temperatures close to 25ºC[9,12,13]. However, the antagonistic relationship between T_{lum} and ΔT_{sol} makes it difficult to simultaneously meet such specifications. In fact, for the particular case of undoped VO_2 monolayers, T_{lum} values hardly exceed 40%, as solar modulations higher than 10% require an optimization of the film thickness. Likewise, issues such as the challenging vanadium chemistry, the narrow reaction window for forming VO_2, the complexity and high cost of the manufacturing processes involved, or the few studies carried out on glass substrates, limit the large-scale industrial transfer of this technology.

In order to fill this gap, our recent work introduced a simple two-step route to attain high-performance VO_2(M1) coatings on glass substrates, which comprises the initial sputtering of 50 nm thick porous vanadium films and the subsequent fast oxidation into an open tube[14] supported on previous optimizations for 700 nm V porous layers[15].

Based on the precise control of the annealing parameters, as well as on the enhancement of reactivity and selectivity linked to the porous structures resulting from the GLancing Angle Deposition (GLAD), different pathways for the synthesis of high-performance VO_2-based coatings with unique thermochromic features for smart window applications were disclosed. Furthermore, the good balance achieved for light transmittance and solar modulation capacity was coupled with unusually low T_c values. They cannot be achieved by elemental doping but rather by the development of oxygen vacancies resulting from the very fast nature of the thermal treatments involved. Nevertheless, it should be noted that this report only covers the effect that reaction temperatures and times have on the oxidation processes of $\alpha = 85^{\circ}$ V-GLAD systems of a same thickness and characteristics (i.e. initially of 50 nm).

The present study complements our previous investigations by offering a more global and complete insight into the fast oxidation of porous vanadium coatings in air thanks to the exhaustive evaluation of the effects of the different parameters involved in the annealing processes as well as the influence of layer thickness and porosity. To meet this goal, V-GLAD layers of 100, 25 and 12.5 nm nominal thickness were deposited on glass substrates. They were subsequently characterized by scanning electron microscopy (SEM) and scanning-transmission electron microscopy (S)TEM techniques. Afterwards, the samples were thermally treated at different temperatures (T_r) and reaction times (t_r) depending on the volume of material to be oxidized. The microstructural and optical characterization of the oxidized systems was carried out by combing SEM and variable temperature Vis-NIR spectrophotometry measurements, shedding light on the effects of layer thickness, the total surface area exposed to oxidation, as well as reaction temperatures and times, on the synthesis of VO_2-based thermochromic coatings of diverse nature, morphology and performance. Likewise, the effect of heating rate was

also investigated. Additionally, a comprehensive optical study was presented for all heat-treated samples, putting a special emphasis on the parameters that determine the viability of the manufactured coatings for smart window applications (T_{lum}, ΔT_{sol}, T_c).

2. Materials and Methods

2.1. Deposition process

Films were deposited at room temperature by DC magnetron sputtering from a vanadium metallic target (51 mm diameter and 99.9 atomic % purity) in a homemade deposition chamber. It was evacuated down to 10^{-5} Pa before each run by means of a turbomolecular pump backed by a primary pump. The target was sputtered with a constant current density J = 100 A m^{-2}, leading to a constant target potential of 312 V. Glass substrates (Menzel Gläser ® microscope slides) were placed at 65 mm from the target center. On the basis of our previous studies[15,16], porous V films with large surface-to-volume ratios and enhanced reactivity to oxidation were deposited by the GLAD technique. The incidence angle (α) of the incoming particle flux relative to the substrate normal was set at α = 85º (the maximum allowed for efficient GLAD deposition, so that the higher the deposition angle, the higher the overall porosity of the film and, therefore, its specific surface area[17]) with no rotation of the substrate (i.e., ϕ = 0 rev h^{-1}). Argon was injected at a mass flow rate of 2.40 sccm and the pumping speed was maintained at S = 13.5 L s^{-1} leading to a sputtering pressure of 0.3 Pa. Different vanadium film thicknesses (12.5, 25 and 100 nm) were achieved by adjusting the deposition time according to an average deposition rate of 240 nm h^{-1}, which was previously determined for α = 85º.

2.2. Thermal treatments

After deposition, vanadium samples were thermally treated in a homemade reaction system. It consists in an Al_2O_3 tube on a SiC resistors furnace being able to reach 1500°C, with an attached concentric steel tube with a high-temperature steel covered K-type thermocouple inside. This thermometer bar acts as an axle for a system of horizontal translation (for a more detailed overview of the reaction system, refer to Supplementary Material Section I). At the end of the metallic tube nearby the furnace, the thermocouple crosses and fixes to a cylinder placed inside this tube, mechanized with a hitch to hang a combustion boat. Thus, the thermometer tip is always placed some millimeters over the center of this alumina crucible, allowing the temperature in the reaction zone to be life-tracked. The other end side also crosses and is fixed to another piece that is part of a handlebar used to slide the specimen holders inside and outside. In this way, by fixing a temperature in the center of the furnace, one is able to control the temperature increase (heating rate) by moving the boat more and more inside the furnace. Consequently, translation routines were prepared for reaching an average heating rate of 42ºC s^{-1}, as well as for adjusting longer or shorter reaction times at a desired temperature. Lastly, all the samples were cooled down in air. It should be noted that the choice of these thermal treatment conditions is grounded in a preliminary study focused on the oxidation of V−GLAD thin films deposited on silicon substrates[15] that evolved from previous studies for the reactivity of vanadium nanoparticles and the achievement of undoped and W-doped M1-VO_2 thermochromic powders[18,19].

2.3. Characterizations

Topographic scanning electron microscopy (SEM) images were acquired using a FEI Nova NanoSEM operating at 5 kV in order to examine the surface morphology of the films before and after each thermal treatment. For the determination of layer

thicknesses, transmission electron microscopy (TEM) experiments were conducted in a Thermo Scientific TALOS F200X G2 analytical microscope operated at 200 kV and equipped with a Super-X windowless energy-dispersive X-ray spectrometry (EDX) system that includes four silicon drift detectors. Local compositional analyses were performed by combining high-angle annular dark-field imaging (HAADF) and EDX acquisitions using the scanning (STEM) mode. Electron-transparent cross-sections were prepared for TEM observations by progressive thinning with a tripod (Model 590 Tripod Polisher®) down to a few microns, followed by Ar^+ ion-milling at an acceleration energy of 3.5 keV in a Gatan Precision Ion Polishing System (PIPS)-691 at ±7º milling angles (double-beam mode). The thermochromic optical behavior of the prepared VO_2 coatings was determined via transmission spectroscopy using an Agilent Cary 5000 spectrophotometer (photometric accuracy ±0.1%) equipped with a custom-made temperature controlled stage. Thus, Vis-NIR transmission spectra of 380–2500 nm were recorded at selected temperatures in the range of 25–90ºC. Additionally, for the dynamic monitoring of the thermally induced phase transition, the temperature evolution of the optical transmittance at a selected NIR wavelength (2000 nm) was observed in both heating and cooling cycles at a controlled rate of 5ºC min^{-1}. DC electrical resistivity *vs.* temperature of the oxidized films (included in the Supplementary Material) were performed in a custom-made chamber. It is covered in order to have a dark environment, using the four-probe van der Pauw geometry in the temperature range of 25–90ºC with a ramp of 1°C min^{-1} and then back to 25°C with the same negative ramp. Humidity and cleanness were considered as constant. The error associated to all resistivity measurements was always below 1% and the quality of the contacts was checked prior to every run (I/V correlation close to 1) to ensure that an ohmic contact was attained (use of gold coated tips).

3. Results and discussion

3.1. Micro- and nanostructural characterization of as-deposited samples

Having studied in depth the thermochromic behavior of the systems resulting from the controlled fast oxidation of V-GLAD samples of 50 nm nominal thickness (τ_N) in air[14], it is now time to explore the effect that layer thickness has not only on the optical performance of the film once oxidized, but also on its reactivity and selectivity when carrying out the thermal treatment. For this purpose, pure vanadium GLAD films of τ_N = 12.5, 25, and 100 nm were deposited on glass substrates at $\alpha = 85°$. **Figure 1** shows the characteristic SEM topography of each of the different deposited samples. Once again, it reveals the strong dependence of porosity on layer thickness for GLAD systems. The higher the layer thickness, the greater the porosity[20]. This fact finds an explanation in the existence of two deposition regimes during deposition at glancing angles, resulting in a mostly porous structure as the shadowing effects begin to prevail over the diffusive ones (the latter is more prominent in the early stages of deposition)[21,22]. For this reason, the surface microstructure of the thicker sample (τ_N = 100 nm) reveals the so-characteristic porous structure of V-GLAD systems (shadow-dominated deposition regime)[15,16], while the thinner ones (τ_N = 12.5 and 25 nm), despite they are also certainly porous, do not exhibit such an evident porosity (diffusion-dominated deposition regime). Therefore, considering that all samples were deposited with the same conditions changing only the deposition time, it becomes clear that the thicker sample should have a greater real thickness than the nominally targeted as a direct consequence of the porosity observed in **Figure 1**.

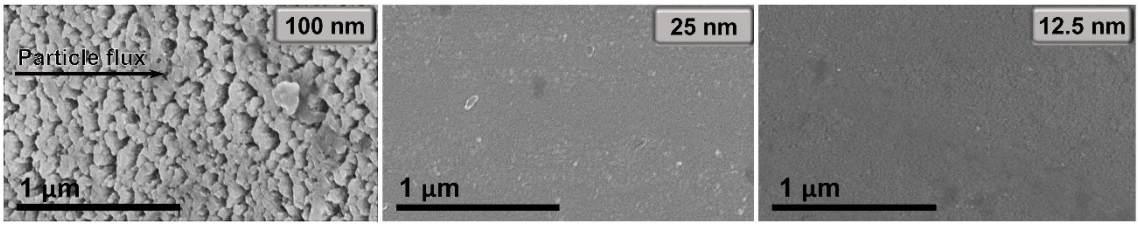

Figure 1. Topographic SEM micrographs of as-deposited vanadium GLAD films. The black arrow indicates the direction of the particle flux during each GLAD deposition.

Additionally, **Figure 2** displays the STEM-EDX elemental analyses carried out in order to disclose the real thickness (τ_R) of as-deposited V-GLAD samples. As can be seen in **Fig. 2(a)**, the high-angle annular dark field (HAADF) micrograph collected for τ_N = 100 nm, in addition to showing a porous structure of inclined columns so characteristic of GLAD systems, reveals layer thicknesses significantly superior to the nominal values. This is in good agreement with what was predicted after SEM observations. By contrast, the identification of the thinner V-GLAD layers (see HAADF nanographs in **Fig. 2(b)** and **(c)**) was more complex (in addition to dealing with much narrower thicknesses, the columnar structure could not be observed in either of the two cases). So it was necessary to perform elemental analyses in order to determine the experimental thicknesses of these samples. In this sense, through the STEM-EDX elemental profiles obtained for V (associated to the deposited film) and Si (belonging to the glass substrate) atoms along the whole coating thickness (**Fig. 2(d–f)**), it was found that the real layer thicknesses (τ_R) for samples deposited at τ_N = 100, 25, and 12.5 nm were approximately $\tau_R \approx$ 180, 24, and 12 nm, respectively. Hence, it is confirmed that the thinner samples (τ_N = 25 and 12.5 nm) are developed under a regime mainly dominated by diffusion between the small islands of material generated during the early stages of deposition, giving rise to nanopores that do not lead to increase the layer thickness.

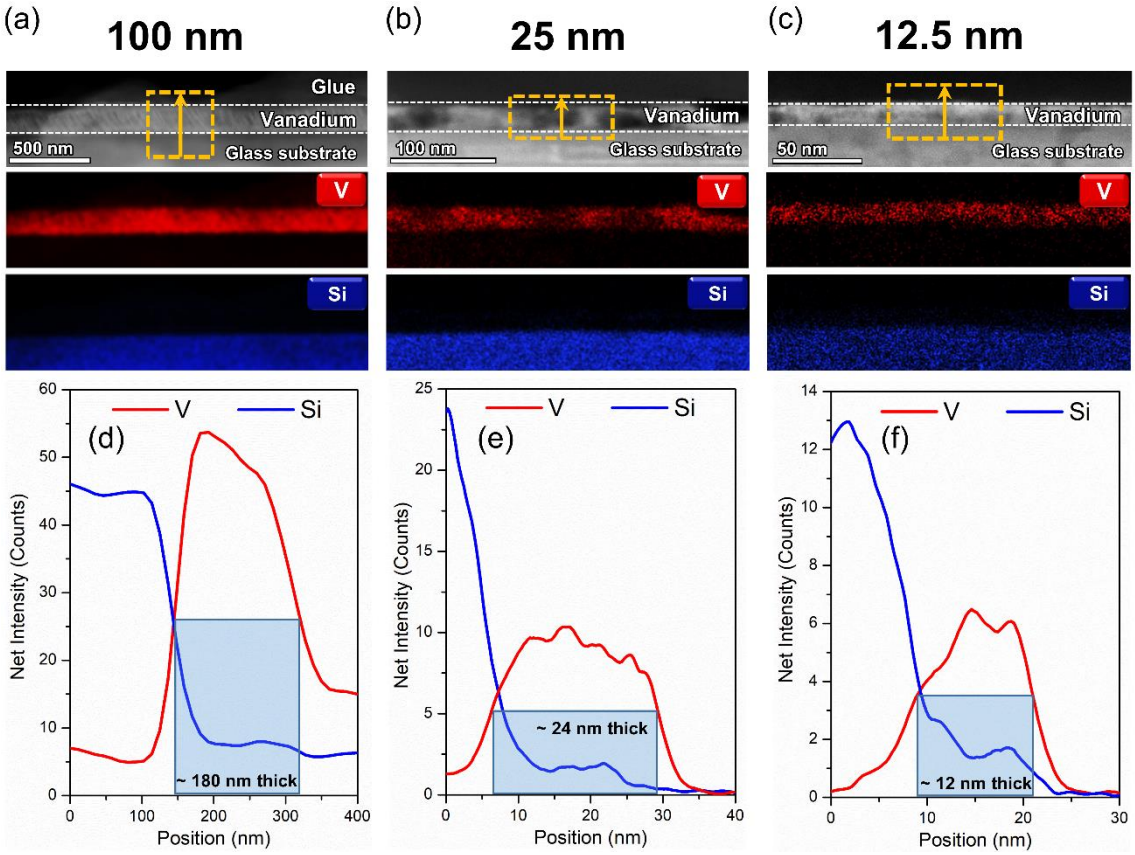

Figure 2. STEM-EDX analyses of as-deposited V-GLAD samples. STEM-HAADF micrographs and elemental maps (V and Si atoms) for samples deposited with (a) 100, (b) 25, and (c) 12.5 nm nominal thickness (τ_N). Integrated elemental line profiles (V and Si atoms) taken along the same imaged coatings and substrate portions. Note that the real thicknesses (τ_R) were extracted from the full width at half maximum values of net intensity from vanadium.

Furthermore, in order to better understand this increase of porosity with thickness, τ_R *vs.* τ_N was plotted and fitted with a polynomial function for the range τ_N =0–100 nm (see Supplementary Material Section II). These results do not only allow us to estimate the real thickness within the addressed τ_N range, but also to determine the threshold thickness when the GLAD deposition regime begins to be dominated by shadowing

effects, which was found to be $\tau_N \approx 26$ nm. From this point forwards, the porosity, and therefore the total thickness of the layer (voids + material), gradually increases. In this context, it must be highlighted that the estimated thickness for $\tau_N = 50$ nm ($\tau_R \approx 62$ nm) is not far from that measured by profilometry in our previous study ($\tau_R = 70 \pm 5$ nm)[14]. Likewise, a rough estimation of the porosity proportion can also be addressed for a given vanadium layer thickness, reaching a maximum value of ~44% for $\tau_N = 100$ nm. Thus, according to our initial assumptions justifying the use of GLAD architectures, the thickest sample is thought to be the most prone to the fast and selective oxidation in air due to its greater specific surface area and, thus, a higher exposure to ambient.

3.2. Oxidized samples

On the basis of former studies, the samples introduced in the previous section were subjected to fast thermal treatments in an open tube at a constant heating rate of ~42ºC s^{-1}, with reaction temperatures (T_r) and times (t_r) varying between 400–550ºC and 1–90 s, respectively, and subsequent instantaneous cooling in air (for a detailed scheme of the fast thermal treatment procedure, refer to Supplementary Material Section III). All these thermal treatments, grouped according to the different V-GLAD layer thicknesses, are listed in **Table 1**. Note that, only nominal layer thicknesses will be referenced in order to simplify and streamline the text. Also, see that the thermal treatment requirements vary significantly for the different τ_N since the optimal combinations of T_r and t_r are highly dependent on the volume of material to be oxidized as well as the total surface area exposed to oxidation.

Table 1. Annealing conditions and nominal thickness (τ_N) of V overlayers for the samples thermally treated in this study. T_r is the reaction temperature and t_r is the reaction time.

Sample	τ_N (nm)	T_r (ºC)	t_r (s)
T100_475_15	100	475	15
T100_475_30			30
T100_475_40			40
T100_475_50			50
T100_475_60			60
T100_475_90			90
T100_550_1		550	1
T100_550_5			5
T100_550_10			10
T25_450_1	25	450	1
T25_475_1		475	1
T25_500_1		500	1
T25_500_5			5
T25_525_1		525	1
T12.5_450_1	12.5	450	1
T12.5_450_5			5
T12.5_475_1		475	1
T12.5_500_1		500	1

3.2.1. Surface microstructure

Structures and morphologies resulting from the rapid annealing of different V-GLAD sample thicknesses were observed by SEM. **Figure 3** shows microstructures (top-view SEM micrographs) that were developed after the thermal treatments carried out on 100 nm V-GLAD samples. They are mainly characterized by the presence of disordered and non-equiaxial grains that grow preferentially along one axial direction as both T_r and t_r increase. It is worth noting that this axial growth is especially promoted for longer oxidation times within the same target temperature (see as an example the micrographs collected for samples T100_475_90 and T100_550_10). It gives rise to dendritic

structures formed by micro-rod bundles, which are representative of vanadium pentoxide[15]. This suggests that the optimal oxidation times for the preferential synthesis of VO_2 should be below 90 s and 10 s for the temperatures of 475ºC and 550ºC, respectively. Surprisingly, the sample T100_550_1 shows considerably larger grain sizes than those observed for T100_475_15. This points out the key role played by the reaction temperature on the performance of instantaneous and selective heat treatments. It is also noteworthy that samples T100_475_60 and T100_550_5 have comparable structures not only in terms of the surface morphologies, but also in terms of their size. This could be related to the existence of two possible optimization pathways, each of them with unique features as observed in counterpart studies[14].

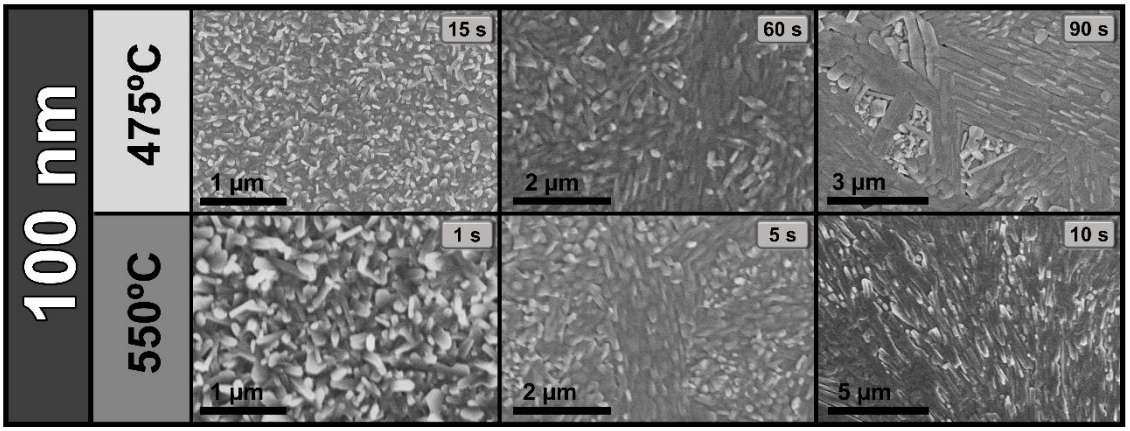

Figure 3. SEM surface topography of 100 nm V-GLAD samples after rapid thermal treatments at T_r = 475ºC and 550ºC, and reaction times (t_r) ranging from 1 to 90 s, as labelled in the images.

On the other hand, **Figure 4** reveals the topographic SEM images collected for 25 nm V-GLAD samples thermally treated at 500ºC and 525ºC for t_r = 1 s. As it can be seen, microstructures are quite different from each other. While sample T25_500_1 exhibits a

homogeneous structure of small and quasi-equiaxed grains, sample T25_525_1 presents a much more heterogeneous topography that combines small and equiaxed grains with bigger and more elongated ones. Therefore, it seems that the reaction temperature acquires a central role in the oxidation process of V-GLAD systems as the layer thickness decreases. As a result, slight temperature variations cause significant changes at the microstructural level, even for very short reaction times. This fact, which could also be related to a significant drop in porosity, leads to define a single optimization pathway for the 25 nm layers. The latter also extends to 12.5 nm thick films. In this connection, it is pertinent to mention that the reason why SEM micrographs of the 12.5 nm samples are not presented here since their thermal treatments always involve short reaction times within a relatively narrow temperature range (450–500ºC). This results in very similar morphologies that do not allow reaching trends and conclusions from a microstructural point of view.

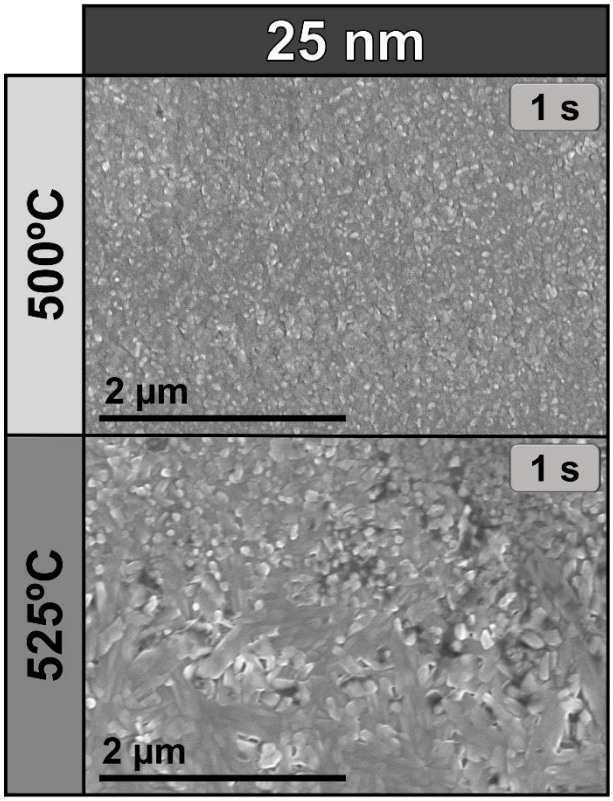

Figure 4. SEM surface topography of 25 nm V-GLAD samples after rapid thermal treatments at T_r = 500ºC and 525ºC, and very short reaction times (t_r) of 1 s before fast cooling, as labelled in the images.

3.2.2. Optical characterization

Vis-NIR transmittance spectra (380–2500 nm) were recorded at 25ºC and 90ºC for all the heat-treated samples in order to evaluate their optical response as well as to qualitatively monitor mixes of vanadium oxides developed from the different reaction conditions (T_r and t_r) and thicknesses. Furthermore, the thermochromic features of these coatings were also quantitatively evaluated through their optical performances. The following characteristics determine their applicability in smart windows: (i) the luminous transmittance, T_{lum}; (ii) the solar modulation ability, ΔT_{sol}; and (iii) the solar modulation in the near infrared, ΔT_{IR}. For all samples, these values are given in **Table 2** (calculated as described by Outón *et al.*[23]).

Table 2. Radiometric (T_{sol}) and photometric (T_{lum}) parameters changes with heating for all studied samples. For a detailed definition and measurements of these parameters, refer to the work of Outón *et al.* (Appendix A)[23]. Accuracy of these values is ±0.1%.

Sample	T_{lum} (%)	ΔT_{lum} (%)	ΔT_{sol} (%)	$\Delta T_{sol.\ rel}$ (%)	ΔT_{IR} (%)	$\Delta T_{IR.\ rel}$ (%)
T100_475_15	18.4	0.5	3.5	18.1	8.7	35.9
T100_475_30	15.9	0.7	5.7	33.6	12.4	57.9
T100_475_40	14.0	2.5	5.5	36.9	9.7	56.1
T100_475_50	26.7	3.3	8.2	28.7	15.7	44.8
T100_475_60	21.6	3.6	9.6	38.3	17.4	56.0
T100_475_90	19.2	1.9	7.7	33.2	15.0	51.1
T100_550_1	16.1	0.6	3.5	20.7	7.3	37.0
T100_550_5	15.1	2.6	7.3	43.1	14.1	68.4
T100_550_10	27.9	2.0	4.8	14.9	9.0	22.7
T25_450_1	53.2	0.7	0.8	1.4	0.8	1.4
T25_475_1	48.7	0.3	1.5	3.1	3.0	6.2
T25_500_1	52.9	0.0	4.7	8.4	11.2	17.0
T25_500_5	53.9	0.1	2.1	3.8	5.0	8.1
T25_525_1	53.8	0.1	0.6	1.0	1.7	2.4
T12.5_450_1	65.3	0.7	0.8	1.2	0.8	1.1
T12.5_450_5	62.3	0.3	0.4	0.6	0.4	0.6
T12.5_475_1	57.8	0.9	1.6	2.8	2.5	4.2
T12.5_500_1	58.7	0.1	0.2	0.4	0.7	1.1

We will first focus on the results obtained for 100 nm thick films (**Figure 5**). For this purpose, the same approach as our former study will be followed[14]. In this framework, based on the trends observed in the V-O phase diagram[24,25] as well as the optical responses previously reported in the literature for different vanadium oxide thin films[26,27], samples will be considered as a certain amount of VO_2(M1) (given the transmittance drops in the NIR for temperatures above 68°C) coexisting with majority or minority mixtures of VO_{2-x} (characterized by moderate solar modulation abilities and higher transmittances in the NIR than in the visible range) and/or VO_{2+x} phases (with higher transmittance values in the visible range than in the NIR and/or maximum transmittance peaks at ~600 nm), with $x > 0$. This insight is also consistent

with what has been previously observed through studies focused on the reactivity of vanadium nanoparticles with oxygen[18]. Similarly, the relative values of solar modulation in the near infrared ($\Delta T_{IR,\,rel}$, which, unlike ΔT_{sol}, are not affected by T_{lum} variations) will be used as an indicator of the VO_2 yields achieved for the annealed films assuming that transmittance drops at infrared wavelengths are solely and exclusively due to the presence of such dioxide. However, this last interpretation must be taken with caution, rather as a comparative criterion between samples, but never as an indicator of the real VO_2 proportion in the sample. In this light, it is observed that 100 nm samples treated at 475ºC (**Fig. 5(a)**) give rise to significant VO_2 yields even for t_r = 15 s, which is particularly surprising considering that identical thermal treatments performed on 50 nm V-GLAD samples led to reaction products much poorer in VO_2[14]. This proves that our initial hypotheses are correct, so that the high VO_2 yields generally observed for 100 nm samples can only be explained by the enhanced reactivity and selectivity resulting from their more porous structure and, therefore, with a greater specific surface (especially favored for thicker GLAD films). However, all of them exhibit the drawback of relatively low visible transmittance values (T_{lum} values between 14–27%). In this context, a slight decrease of the visible transmittance can be appreciated when increasing t_r from 15 to 40 s. It may be associated with a progressive increase of the VO_2 amount (note that these visible transmittance values are one order of magnitude higher than those previously reported for what was claimed as a pure VO_2 coating with a similar thickness[28,29]). Besides, the greater transmittances in the NIR than in the visible range observed for samples T100_475_15/30/40 make us think that they are mainly composed of VO_2 coexisting with VO_{2-x} phases (to see the transmittance spectra of sample T100_475_30 at 25ºC and 90ºC, refer to Supplementary Material Section IV).

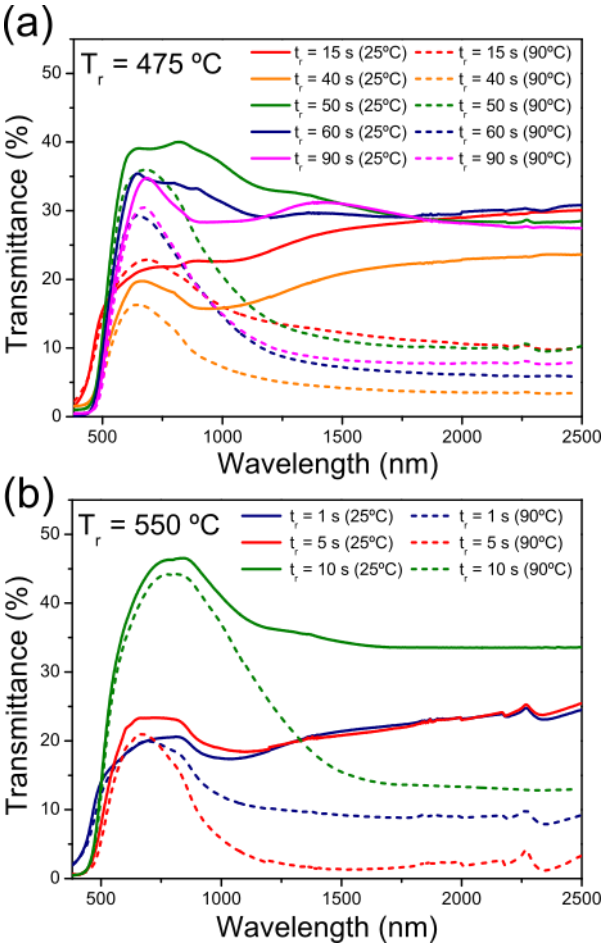

Figure 5. Transmittance spectra recorded at 25ºC (solid lines) and 90ºC (dashed lines) for 100 nm thick samples thermally treated at (a) 475ºC and (b) 550ºC for a reaction time t_r ranging from 1 to 90 s.

Conversely, reaction times above 40 s give rise to a majority of VO_2 + VO_{2+x} phase mixture (characterized by lower transmittances in the NIR than in the visible), leading to a kind of pseudo balance in the quantities of VO_2 generated. The remaining amounts of VO_{2-x} further oxidize to VO_2 + VO_{2+x}, while the part of previously generated VO_2 stay unreacted and part gives way to the progressive formation of VO_{2+x} mixtures. This explains the $\Delta T_{IR.\,rel}$ values obtained for samples oxidized at t_r = 40–90 s that remain almost stable in comparison with the maximum obtained for t_r = 30 s in this 475ºC

series (**Table 2**). Similarly, it is also observed that the modulation of solar radiation becomes maximum for this t_r = 60 s (ΔT_{sol} = 9.6%). This comes along with an increase of the luminous transmittance (T_{lum} = 21.6%), although still far below those required for smart window applications. This latter could be associated to the rise of V_6O_{13} phase, a compound characterized by its high transmittance in the visible range[30], which is suspected to reach its peak at t_r = 50 s (maximum values of transmittance at 380–780 nm), and whose generated quantities would be gradually consumed to form VO_{2+x} mixtures (note that the peak signatures of the transmittance spectra recorded for mixtures of VO_2 and V_2O_5[31] are quite similar to those found for the sample treated at t_r = 90 s). Furthermore, such T_{lum} values could also be associated with changes in the microstructure of the coatings (rising in overall porosity) as t_r and T_r increase (see **Fig. 3**), so that the higher the porosity, the higher the transmittance. Also noteworthy are the variations of luminous transmittance (ΔT_{lum}) experienced by these samples. Transmittance increases progressively until reaching a maximum at t_r = 60 s (ΔT_{lum} = 3.6%), after which it considerably reduces. This phenomenon, previously observed in the literature[31,32], has not yet been attributed to a specific cause. It substantially contributes to the remarkable ΔT_{sol} values calculated for samples T100_475_50/60, being in turn closely related to the the solar irradiation becomes maximum at visible wavelengths.

Instead, the spectra obtained for 100 nm V-GLAD samples oxidized at 550°C (**Fig. 5(b)**) show a maximum VO_2 yield for t_r = 5 s ($\Delta T_{IR.\,rel}$ = 68.4%), which is accomplished thanks to the almost direct transformation of V into VO_2. So the formation of this compound is favored over other vanadium oxides (the film receives a quasi-instantaneous supply of energy which is mostly used for the selective synthesis of VO_2). However, it should be noted that the solar modulation capacity of the T100_550_5

sample is not as high as those reached for the T100_475_50/60 samples. This can be explained by its lower T_{lum} variation on heating (ΔT_{lum} = 2.6%). Beyond that, similar trends to those noticed for 475°C treatments are observed, although with certain nuances linked to the considerable reduction in the reaction time window: an initial phase of progressive enrichment in VO_2 (t_r between 1–5 s) leading to T_{lum} values below 16.1%, followed by a second phase in which the system experiences a decrease in VO_2 quantities ($\Delta T_{IR.\,rel} \approx 23\%$). This is gradually consumed to generate a majority of VO_{2+x} mixtures with improved T_{lum} values (sample T100_550_10). This demonstrates that reactions carried out at 550°C progress so rapidly that optimal balances of pseudo-equilibrium states cannot be reached.

Some similar patterns happen for thermal treatments carried out on the thinner films. The volume of material to be oxidized is smaller and reaction times longer than one second lead to the formation of predominant oxygen-enriched mixtures (O/V > 2) even for temperatures below 525ºC. It seems clear that the reaction temperature plays a more pivotal role in oxidation processes of V-GLAD films as the layer thickness decreases. This easy to guess hypothesis is confirmed through the outcomes obtained for samples of 25 and 12.5 nm nominal thickness. **Figure 6(a)** shows the Vis-NIR transmittance spectra recorded at 25ºC and 90ºC for 25 nm thick films treated at t_r = 1 s with T_r ranging from 450ºC to 525ºC. As can be seen, temperature variations of 25ºC imply substantial changes in the spectra obtained for instantaneous reactions, which in turn is related to the development of different vanadium oxides. It should also be noted that all these samples exhibit improved visible transmittance values (T_{lum} values between 48–54%), although this would be more a consequence of the decrease in thickness than of the synthesized oxides. Moreover, the shape of these spectra shows a progressive enrichment in VO_2 of initial VO_{2-x} mixtures as T_r increases from 450ºC to 500ºC.

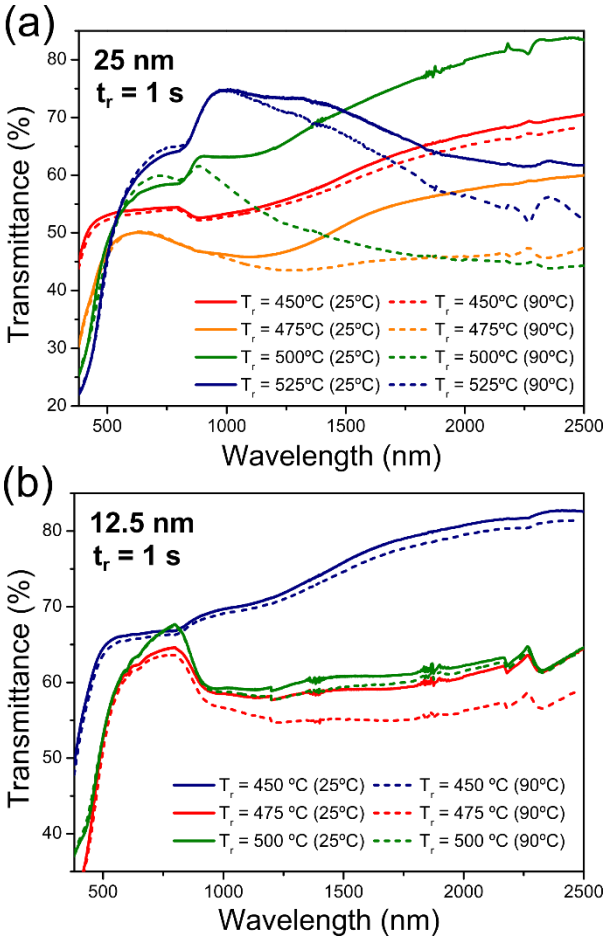

Figure 6. Transmittance spectra recorded at 25ºC (solid lines) and 90ºC (dashed lines) for (a) 25 nm and (b) 12.5 nm thick samples thermally treated during 1 s for a reaction temperature T_r ranging from 450ºC to 525ºC.

Conversely, higher temperatures lead to a decrease in VO_2 yields in favor of the formation of VO_{2+x} phase mixture. A similar effect also occurs when the reaction time is slightly increased for $T_r \leq 500$°C (to see the transmittance spectra of sample T25_500_5 at 25ºC and 90ºC, refer to Supplementary Material Section IV). Therefore, and in view of the above, one could say that sample T25_500_1 is the most interesting one, not only for its higher VO_2 yield in this series ($\Delta T_{IR.\,rel}$ = 17.0%) but also for the remarkable balance achieved for the parameters T_{lum} and ΔT_{sol} (52.9% and 4.7%, respectively),

which makes it a suitable candidate for smart window applications. In this sense, it should be highlighted that, although it is rather moderate when compared to those achieved for 100 nm thick samples, this ΔT_{sol} value is quite worthy. Thickness of this produced VO_2 layer is much more limited, as well as the low ΔT_{lum} values registered for the thinnest samples (it must be remembered that variations in luminous transmittance lead to significantly higher ΔT_{sol} values). Thus, it seems that such T_{lum} variations are related to the pseudo-equilibrium states reached in the oxidation processes for longer reaction times. On another note, the great T_{lum} value achieved for sample T25_500_1 could be associated either with the formation of VO_2 + V_6O_{13} phases (the latter with high transmittance in the Vis-NIR range), and/or with the arising of porosity as a consequence of the microstructural changes induced in the film by the thermal treatment.

Figure 6(b) reveals the transmittance spectra recorded for 12.5 nm thick V-GLAD samples subjected to instantaneous annealing. Further reductions in layer thickness lead to significant improvements in visible transmittances (T_{lum} values between 57–66%). However, the price to pay here is a substantial drop in the solar modulation ability of such systems (ΔT_{sol} < 1%). It can be due to either (i) the volumes of VO_2 attained are so small that they do not produce significant thermochromic effects (the observed $\Delta T_{IR.\ rel}$ < 4% supports this idea); or (ii), at these thicknesses, the V-GLAD film behaves as a compact non-porous film, undermining the selectivity and reactivity of the thermal treatments carried out and, thus, hindering the synthesis of VO_2. The latter would explain the main formation of VO_{2-x} when operating at 450ºC, and the subsequent development of majority amounts of VO_{2+x} at $T_r \geq 475$ºC, which coexist together with certain, but still insufficient, amounts of VO_2. Similarly, thermal treatments were also carried out at 450ºC for t_r = 5 s (to see the transmittance spectra of sample T12.5_450_5

at 25ºC and 90ºC, refer to Supplementary Material Section IV). Nevertheless, these results are quite similar to those obtained for sample T12.5_450_1. This shows that reactions giving rise to the VO_2 compound take place at temperatures above 450ºC. None of the samples showed either a remarkable optical response or any other particularity, so it was decided to put an end to the studies for the layers of τ_N = 12.5 nm.

At this point, the importance of layer thickness and porosity in the rapid and selective annealing of V-GLAD thin films in an air atmosphere has been demonstrated. Nonetheless, there is also another parameter playing a fundamental role in oxidation processes: the heating rate. Through an additional study that deals with the definition of a constant that collects the contribution of all the parameters involved in the thermal treatment of V-GLAD systems for different layer thicknesses (see Supplementary Material Section V), the minimum heating rate requirements to maximize VO_2 yields were estimated based on two flash annealing scenarios at 500ºC: a first one, rather ideal, in which the cooling is considered to take place instantaneously; and a second one in which the sample is cooled down in air atmosphere (the same case as the one addressed in the present study). Results obtained for both scenarios underline the vital role of working at higher heating rates when decreasing the layer thickness, to the point of becoming the critical thermal treatment parameter for layer thicknesses below 50 nm. Additional calculations were also performed to find out the optimal temperature range for heat treatment of 12.5 nm thick layers, leading to temperatures similar to those determined experimentally (refer to Supplementary Material Section V).

It seems clear that there are two optimal routes for the fabrication of high performance VO_2-based coatings. A first one for 100 nm V-GLAD samples comprises the formation of mainly VO_2 + VO_{2+x} phase mixture after reaching pseudo-equilibrium states at

475°C and t_r = 40–60 s. The second one for 25 nm thick samples involves the instantaneous transformation of V into majority fractions of VO_2 at 500°C and t_r = 1 s. To have a better insight into the features of the MIT for samples attained through these two pathways, the kinetic evolution of the transmittance at 2000 nm was monitored for samples T100_475_40/50/60 (**Figure 7**) and T25_500_1 (**Figure 8**) during consecutive cycles of heating and cooling at a constant rate. **Table 3** lists the transition temperatures, on heating ($T_{c(H)}$) and on cooling ($T_{c(C)}$), calculated from the derivative curves of the transmittance plots by fitting them to Gaussian functions and considering the peaks as the temperature of the minima variation rate (**Fig. 7(b–d)** and inset in **Fig. 8**), along with the hysteresis loop width (W_H), transmittance at 2000 nm for 25ºC (T_{max}) and for 90ºC (T_{min}), and their relative difference.

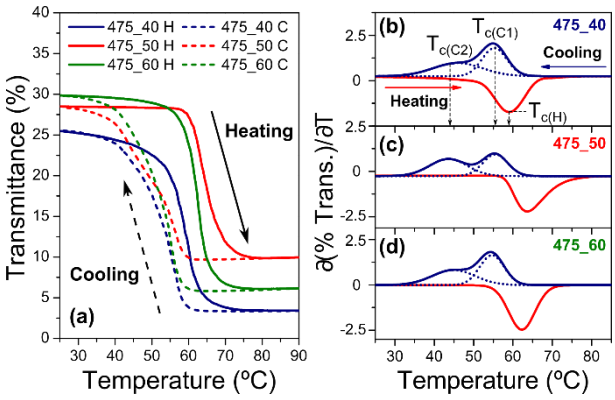

Figure 7. (a) Thermal evolution of the optical transmittance of T100_475_40 (blue), T100_475_50 (red), and T100_475_60 (green) samples at 2000 nm on heating (solid lines) and cooling (dashed lines). Derivative of each kinetic thermochromic cycle for samples (b) T100_475_40, (c) T100_475_50, and (d) T100_475_60 on heating (red) and cooling (blue). For a better overview, the derivatives of the cooling are plotted in absolute values, so that the minima and maxima indicate the T_c at heating (H) and cooling (C), respectively.

Figure 7 shows a feature common to the three most interesting samples of the T100_475 series: the development of asymmetric hysteresis loops leading to two different transition temperatures for the cooling cycle. These temperatures have been denoted $T_{c(C1)}$ and $T_{c(C2)}$ to refer to high and low $T_{c(C)}$, respectively. However, although all these samples exhibit very similar values of $T_{c(C1)}$ and $Tc_{(C2)}$, with minimum variation rates (absolute minimum of the derivatives of the optical hysteresis during cooling cycles) at $T_{c(C1)}$ = 55ºC, relevant differences can be appreciated in the two slopes defining the hysteresis all of them for the cooling stage. In this sense, a maximum splitting of the peaks associated with $T_{c(C1)}$ and $T_{c(C2)}$ is observed for t_r = 50 s (**Fig. 7(c)**). This results in the appearance of two clearly defined hysteresis slopes (see sample T100_475_50 in **Fig. 7(a)**). On the contrary, reaction times above 50 s tend to merge both peaks. Something similar occurs for the transition temperatures for the heating cycle, again with sample T100_475_50 breaking the natural trend whereby longer oxidation times result in shifts in $T_{c(H)}$ towards higher values, but always below those reported for pure VO_2 films (~ 68ºC). The combined action of these two occurrences results in a maximum variable hysteresis width for the sample T100_475_50 (W_H = 9–20ºC). Furthermore, the way in which these events take place leads us to believe that they are related to the rise of an intermediate oxide between VO_2 and V_2O_5, most likely V_6O_{13}, for t_r = 40–50 sec. Notwithstanding, this latter should not be misinterpreted as the root cause of the asymmetric hysteresis in vanadium dioxide thin films, which is linked, in agreement with what was previously observed in the SEM micrographs of oxidized samples, to the existence of VO_2 crystals with different grain sizes[33].

Table 3. Main features of the thermochromic hysteresis loops illustrated in **Fig. 7** and **Fig. 8**: $T_{c(H)}$ denotes the temperatures of the MIT for heating; $T_{c(C1)}$ and $T_{c(C2)}$ indicate the temperatures of the MIT for cooling; W_{h1} and W_{h2} are the hysteresis loop widths given by $T_{c(H)} - T_{c(C1)}$ and $T_{c(H)} - T_{c(C2)}$, respectively; T_{max}, and T_{min} denote the 2000-nm wavelength transmittances at 25ºC and 90 ºC; and ΔT_{rel} is the relative decrease in the transmittance upon the transition at 2000 nm. Accuracy of the temperature (ºC) and transmittance (%) values are ±0.5 and ±0.1%, respectively.

Sample	**T_c (ºC) heating**	**T_c (ºC) cooling**		**W_h (ºC)**		**T_{max} (%)**	**T_{min} (%)**	**ΔT_{rel} (%)**
		C1	**C2**	**1**	**2**			
T100_475_40	59	55*	46	4	13	25.5	3.4	86.7
T100_475_50	64	55*	44	9	20	28.5	9.9	65.3
T100_475_60	62	55*	45	7	17	29.9	6.1	79.6
T25_500_1	53	42	–	11	–	79.9	45.4	43.2

* Main peak

ΔT_{rel} values highlight the particularly high VO_2 performances for the samples T100_475_40 and T100_475_60, which is characteristic of the above mentioned pseudo-equilibrium state. When all outcomes obtained for thermal treatments carried out at 475ºC for 100 nm thick V-GLAD samples are put together, it is concluded that the T100_475_60 sample is the one with the most interesting attributes: (i) an extraordinary ΔT_{sol} value of 9.6%; (ii) a higher visible transmittance compared to those obtained for the other oxidized samples of the same thickness; and (iii) a MIT 6ºC below the conventional value reported for pure VO_2 during the heating stage, surprisingly being achieved without doping. To better understand the joint evolution of these three properties during the heating-cooling cycle, **Figure 9(a)** shows the Vis-NIR transmission spectra of sample T100_475_60 gradually increasing or decreasing the temperature.

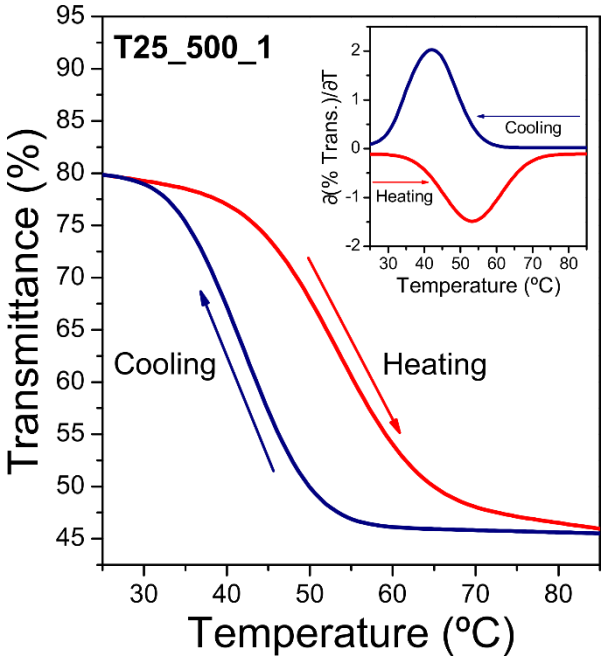

Figure 8. Thermal evolution of the optical transmittance of T25_500_1 for sample T25_500_1 at 2000 nm during heating (red) and cooling (blue) cycles. The inset shows the derivative of each kinetic thermochromic cycle (the derivatives of the cooling are plotted in absolute values).

On the other hand, the thermal evolution of transmittance experienced by sample T25_500_1 during heating and cooling cycles, as well as the associated derivatives (**Fig. 8**), reveal a rather different optical behavior. This is characterized by an almost symmetric hysteresis loop leading to unique values of T_c when increasing and decreasing temperature and, thus, a constant hysteresis width of 11ºC. Also noteworthy is its surprising drop in $T_{c(H)}$, which turned out to be 15ºC below the normal value for undoped VO_2 samples. This result is a direct consequence of the thermal treatments combined with GLAD vanadium addressed in this study. Oxidation reactions occur so rapidly that stoichiometry just of O/V = 2 cannot be completely reached, leading to the appearance of oxygen-deficiency-related defects (previously reported to be responsible

for the drops in T_c[34,35]). Indeed, it should be noted that the transmittance spectra recorded for sample T25_500_1 are quite similar to those reported by Chen *et al.* for a substoichiometric compound described as $VO_{1.963}$[35]. Likewise, in agreement with the trends observed throughout this study, it can be determined that this effect becomes more accentuated for shorter reaction times. Hence, to the initial attractiveness of the good balance of T_{lum} and ΔT_{sol} achieved for the samples synthesized through this second instantaneous annealing route, we must add the remarkable drop of T_c values. This was often observed for doped samples[36,37], and has no negative impact on the optical performance of the coatings. All of these attributes are simultaneously highlighted in **Fig. 9(b)**, where transmission spectra *vs.* wavelength of sample T25_500_1 collected at multiple temperatures during heating-cooling cycles are displayed.

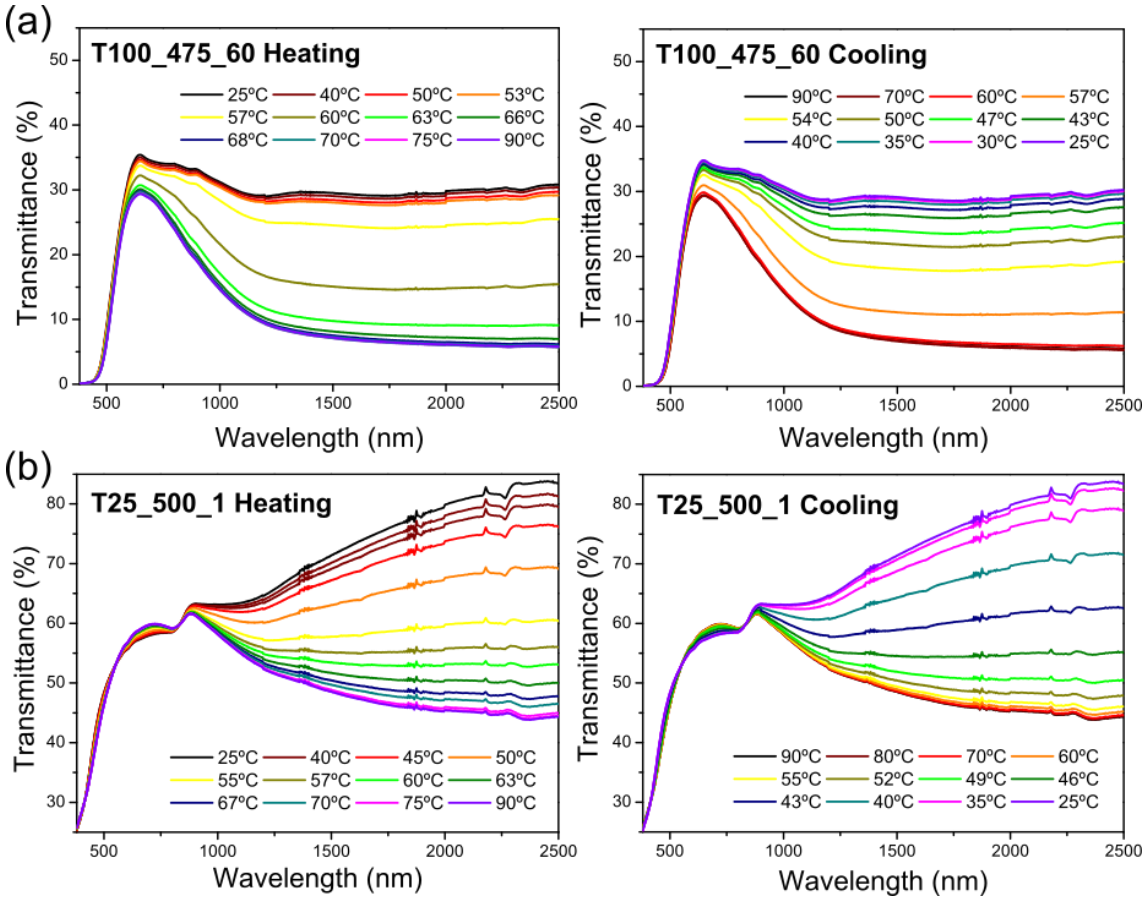

Figure 9. Vis-NIR transmission spectra of samples (a) T100_475_60 and (b) T25_500_1 recorded gradually increasing (left) or decreasing (right) the temperature.

Figure 10 summarizes the results obtained for 100 and 25 nm thick V-GLAD samples based on values that determine the thermochromic performance of smart glazing (ΔT_{sol}, T_{lum} and T_c) for different temperatures and oxidation times. This overview allows us to appreciate how the increase in VO_2(M1) yields, which has a direct incidence on the increase of ΔT_{sol} values, translates into remarkable decreases of T_{lum} values for $t_r \leq 30$ s. Instead, reaching pseudo-equilibrium states (t_r = 40–60 s for 100 nm samples treated at 475ºC) enable the simultaneous increase of T_{lum} and ΔT_{sol} values. However, although the solar modulation ability of these coatings is outstanding, their low visible transmittance still limits their application for smart windows. In any case, the outcomes

obtained for the first optimization pathway lead us to think that these systems would be suitable for applications such as translucent glazing, providing natural thermal conditioning in environments where the privacy of people must be safeguarded; or in other fields such as sensors[38,39] or switching electronics[40,41]. In this connection, the suitability of samples T100_475_50 and T100_475_60 for applications as resistive switching electronics was supported by the outcomes attained in resistivity *vs.* temperature measurements (for an in-depth analysis and discussion on these results, refer to Supplementary Material Section VI).

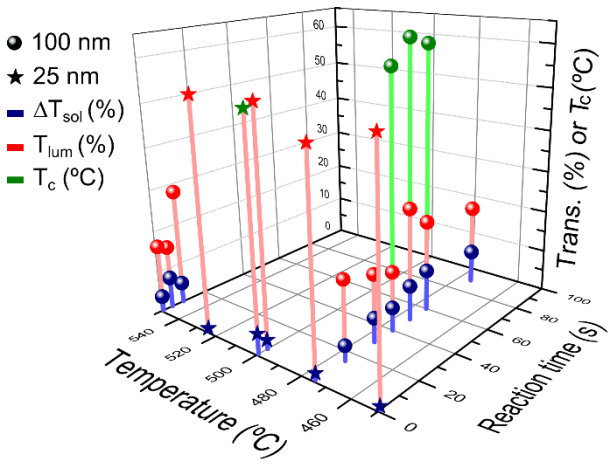

Figure 10. Summary of the thermochromic performances achieved for oxidized 100 and 25 nm thick V-GLAD films (ΔT_{sol}, $T_{lum,}$ and T_c) as a function of the oxidation temperature (T_r) and time (t_r). The transition temperature T_c values referred here correspond to those extracted from the heating cycle ($T_{c(H)}$). The z-axis returns simultaneously the percentage of transmittance (ΔT_{sol} and T_{lum} outputs) as well as the temperature (T_c outputs). Also note that T_{lum} and T_c values for sample T25_500_1 are overlapped (green star).

On the contrary, the 25 nm thick samples, although experiencing significant decreases in ΔT_{sol}, exhibit quite remarkable T_{lum} values. In addition to the natural and significant drop in T_c values as the oxidation time decreases considerably, this makes the T25_500_1 sample a real potential seed for smart glazing applications. Besides, if the negative effect coming from the substrate used in this study is neglected (T_{lum} = 82.1% and T_{sol} = 83.5% for uncoated glass), this sample reaches maximum T_{lum} and ΔT_{sol} values of 64.4% and 5.4, respectively (for more information, see Supplementary Material Section VII). Also note that the balance of T_{lum}, ΔT_{sol} and T_c achieved through the second optimization route is quite remarkable when compared to the those attained so far for undoped single-layer VO_2 coatings[14,23,42–45], which exhibit solar modulation abilities generally below 12% and luminous transmittances hardly exceeding 60–70%, as can be seen in **Table 4**. This becomes even more relevant when considering the advantages of the fabrication strategy described in this work (reaction in the absence of reactive gases or catalysts and no special vacuum or pressure requirements).

Table 4. Comparative study on some of the T_{lum}, ΔT_{sol} and T_c values reported so far in the literature for the fabrication of undoped single-layer VO_2 coatings.

Source	Layer thickness (nm)	T_{lum} (%)	ΔT_{sol} (%)	T_c (heating) (ºC)
Dou *et al.*[45]	30±5	68.2	11.7	~75
Outón *et al.*[23]	40–50	77.6	6.7	76
Zhang *et al.*[44]	~84	~40	NP*	~56
Dietrich *et al.*[43]	~80	~35	~6	~65
Kang *et al.*[42]	43	~60	6.4	NP*
Santos *et al.*[14]	70±5	41.9	8.4	63

*Not provided

Overall, although these simple and cost-effective methodologies are expected to pave the way towards the large-scale manufacture of VO_2 coatings for use in smart glazing. It

should not be forgotten that these results are preliminary. Lowering the critical temperature to around 25°C or increasing the visible transmittance would be some of the upcoming challenges. In this connection, several studies dealing with W-doping strategies prior to similar thermal treatments[18,19] and the deposition of TiO_2 antireflective coatings[46] have proven to be suitable solutions while being compatible with the procedures described in this work, which opens up new avenues for future improvements.

4. Conclusions

The combined effects of layer thickness and porosity as well as the different parameters involved in fast annealing processes leading to the attainment of VO_2-based coatings through the post-deposition selective oxidation of vanadium films sputtered at glancing angles have been extensively investigated. For this purpose, V-GLAD films of different thickness and porosity degree were deposited and subsequently oxidized at different temperatures and reaction times. The characterization of the resulting microstructures as well as their optical responses allowed us to identify the incidence of parameters involved in these procedures. On the one hand, as conventionally observed for GLAD deposition, larger layer thicknesses lead to the fabrication of more porous systems, which have been shown to improve reactivity and selectivity for obtaining the VO_2 compound. However, as the layer thickness increases, the visible transmittance becomes compromised. Conversely, thinner films lead to barely porous structures, which considerably undermines the achievement of high VO_2 yields. To counteract this effect, flash annealing is required, with high heating rates playing an increasingly key role as the layer thickness is reduced. Even so, very poor VO_2 yields are accomplished for V-GLAD thicknesses below 25 nm.

All these studies also allowed us to disclose two optimal pathways for synthesizing high-performance VO_2-based coatings with unique characteristics: (i) a first one at 475ºC and a reaction time t_r = 40–60 s, ideal for thicker samples with thicknesses around 100 nm, which implies reaching pseudo-equilibrium states with the formation of predominant VO_2 + VO_{2+x} phase mixtures; and (ii) a second one for 25 nm thick samples leading to a more direct transformation of vanadium into substoichiometric dioxide thanks to instantaneous reactions (t_r = 1 s) carried out at 500ºC. Regarding the applicability of these systems, it should be noted that the samples obtained through the first optimization route show high modulation capacities (ΔT_{sol} = 5–10%) but very reduced light transmission (T_{lum} = 19–27%), which limits their application in smart glazing. Notwithstanding, the attractive balance of T_{lum} and ΔT_{sol} achieved through the second optimization pathway, coupled with the remarkable drop of the transition temperature T_c (undoped) on heating up to 15ºC below the normal value reported for pure VO_2 (~68ºC), which is associated with oxygen-deficiency-related defects consequence of such instantaneous reactions, make the systems attained by this pathway potentially applicable in energy-efficient smart coatings, even improving the results obtained in our previous studies[14]. This becomes even more relevant when considering the simplicity and cost-effectiveness of the synthesis strategy described in this work (green-like reactions without assistance of reactive gases or catalysts, and no special vacuum or pressure requirements). So it is expected to pave the way for further initiatives towards the large-scale manufacturing of thermochromic VO_2 films.

Acknowledgements

A. J. Santos would like to thank the University of Cádiz and the Spanish Ministerio de Universidades for the concession of a “Margarita Salas” postdoctoral fellowship funded by the European Union - NextGenerationEU (sol-202100211960-tra). J. Outón acknowledges the support by the Spanish Ministerio de Educación y Cultura through grant FPU19-02638. University of Cádiz and IMEYMAT are also acknowledged by financing the mutual facilities available at the UCA R&D Central Services (SC-ICYT), the UCA project references “PUENTE PR2020-003” and “OTRI AT2019/032”, and the IMEYMAT project reference “LÍNEAS PRIORITARIAS PLP2021120-1”. This work was supported by the Spanish State R&D project (Retos y Generación de Conocimiento) ref. PID2020–114418RBI00. The regional government of Andalusia with FEDER co-funding also participates through the projects AT-5983 Trewa 1157178 and FEDER-UCA18-10788. This work was partly supported by the french RENATECH network, FEMTO-ST technological facility, by the Region Bourgogne-Franche-Comté and by EIPHI Graduate School (Contract “ANR–17–EURE–0002”).

Data availability statement

The raw/processed data required to reproduce these findings cannot be shared at this time due to technical or time limitations.

Declaration of Competing Interest

The authors declare that they have no known competing financial interests or personal relationships that could have appeared to influence the work reported in this paper.

REFERENCES

[1] H. Lu, S. Clark, Y. Guo, J. Robertson, The metal-insulator phase change in vanadium dioxide and its applications, J. Appl. Phys. 129 (2021) 240902. doi:10.1063/5.0027674.

[2] Z. Shao, X. Cao, H. Luo, P. Jin, Recent progress in the phase-transition mechanism and modulation of vanadium dioxide materials, NPG Asia Mater. 10 (2018) 581–605. doi:10.1038/s41427-018-0061-2.

[3] M. Chikanari, T. Kanki, T. Wei, H. Tanaka, Enhancement of electronic-transport switching in single-crystal narrower VO_2 nanowire channels through side-gate electric fields, Appl. Phys. Lett. 113 (2018) 053102. doi:10.1063/1.5042674.

[4] K. Dong, H.S. Choe, X. Wang, H. Liu, B. Saha, C. Ko, Y. Deng, K.B. Tom, S. Lou, L. Wang, C.P. Grigoropoulos, Z. You, J. Yao, J. Wu, A 0.2 V micro-electromechanical switch enabled by a phase transition, Small. 14 (2018) 1703621. doi:10.1002/smll.201703621.

[5] T. Driscoll, H.T. Kim, B.G. Chae, M. Di Ventra, D.N. Basov, Phase-transition driven memristive system, Appl. Phys. Lett. 95 (2009) 043503. doi:10.1063/1.3187531.

[6] A. Hendaoui, N. Émond, M. Chaker, É. Haddad, Highly tunable-emittance radiator based on semiconductor-metal transition of VO_2 thin films, Appl. Phys. Lett. 102 (2013) 061107. doi:10.1063/1.4792277.

[7] G. Savorianakis, K. Mita, T. Shimizu, S. Konstantinidis, M. Voué, B. Maes, VO_2 nanostripe-based thin film with optimized color and solar characteristics for smart windows, J. Appl. Phys. 129 (2021) 185306. doi:10.1063/5.0049284.

[8] A.C. García-Wong, D. Pilloud, S. Bruyère, S. Mathieu, S. Migot, J.F. Pierson, F. Capon, Oxidation of sputter-deposited vanadium nitride as a new precursor to achieve thermochromic VO_2 thin films, Sol. Energy Mater. Sol. Cells. 210 (2020) 110474. doi:10.1016/j.solmat.2020.110474.

[9] Y. Cui, Y. Ke, C. Liu, Z. Chen, N. Wang, L. Zhang, Y. Zhou, S. Wang, Y. Gao, Y. Long, Thermochromic VO_2 for energy-efficient smart windows, Joule. 2 (2018) 1707–1746. doi:10.1016/j.joule.2018.06.018.

[10] S. Wang, M. Liu, L. Kong, Y. Long, X. Jiang, A. Yu, Recent progress in VO_2 smart coatings: Strategies to improve the thermochromic properties, Prog. Mater. Sci. 81 (2016) 1–54. doi:10.1016/j.pmatsci.2016.03.001.

[11] T.C. Chang, X. Cao, S.H. Bao, S.D. Ji, H.J. Luo, P. Jin, Review on thermochromic vanadium dioxide based smart coatings: From lab to commercial application, Adv. Manuf. 6 (2018) 1–19. doi:10.1007/s40436-017-0209-2.

[12] N. Shen, S. Chen, R. Huang, J. Huang, J. Li, R. Shi, S. Niu, A. Amini, C. Cheng, Vanadium dioxide for thermochromic smart windows in ambient conditions, Mater. Today Energy. 21 (2021) 100827. doi:10.1016/j.mtener.2021.100827.

[13] X. Cao, T. Chang, Z. Shao, F. Xu, H. Luo, P. Jin, Challenges and opportunities toward real application of VO_2-based smart glazing, Matter. 2 (2020) 862–881. doi:10.1016/j.matt.2020.02.009.

[14] A.J. Santos, N. Martin, J. Outón, E. Blanco, R. García, F.M. Morales, A simple two-step approach to the manufacture of VO_2-based coatings with unique thermochromic features for energy-efficient smart glazing (under review in Energy Build).

[15] A.J. Santos, B. Lacroix, M. Domínguez, R. García, N. Martin, F.M. Morales, Controlled grain-size thermochromic VO_2 coatings by the fast oxidation of sputtered vanadium or vanadium oxide films deposited at glancing angles, Surf. Interfaces. 27 (2021) 101581. doi:10.1016/j.surfin.2021.101581.

[16] V. Collado, N. Martin, P. Pedrosa, J.Y. Rauch, M. Horakova, M.A.P. Yazdi, A. Billard, Temperature dependence of electrical resistivity in oxidized vanadium films grown by the GLAD technique, Surf. Coat. Technol. 304 (2016) 476–485. doi:10.1016/j.surfcoat.2016.07.057.

[17] A.J. Santos, B. Lacroix, F. Maudet, A. Corvisier, F. Paumier, C. Dupeyrat, T. Girardeau, R. García, F.M. Morales, Surface oxidation of amorphous Si and Ge slanted columnar and mesoporous thin films: Evidence, scrutiny and limitations for infrared optics, Appl. Surf. Sci. 493 (2019) 807–817. doi:10.1016/j.apsusc.2019.07.064.

[18] F.M. Morales, M. Escanciano, M.P. Yeste, A.J. Santos, Reactivity of vanadium nanoparticles with oxygen and tungsten, Nanomaterials. 12 (2022) 1471. doi.org/10.3390/nano12091471.

[19] A.J. Santos, M. Escanciano, A. Suárez-Llorens, M. Pilar Yeste, F.M. Morales, A novel route for the easy production of thermochromic VO_2 nanoparticles, Chem. - A Eur. J. 27 (2021) 16662–16669. doi:10.1002/chem.202102566.

[20] F. Maudet, B. Lacroix, A.J. Santos, F. Paumier, M. Paraillous, S. Hurand, A. Corvisier, C. Marsal, B. Giroire, C. Dupeyrat, R. García, F.M. Morales, T. Girardeau, Optical and nanostructural insights of oblique angle deposited layers applied for photonic coatings, Appl. Surf. Sci. 520 (2020) 146312. doi:10.1016/j.apsusc.2020.146312.

[21] A. Barranco, A. Borras, A.R. Gonzalez-Elipe, A. Palmero, Perspectives on oblique angle deposition of thin films: From fundamentals to devices, Prog. Mater. Sci. 76 (2016) 59–153. doi:10.1016/j.pmatsci.2015.06.003.

[22] M.M. Hawkeye, M.J. Brett, Glancing angle deposition: Fabrication, properties, and applications of micro- and nanostructured thin films, J. Vac. Sci. Technol. A Vacuum, Surfaces, Film. 25 (2007) 1317. doi:10.1116/1.2764082.

[23] J. Outón, E. Blanco, M. Domínguez, H. Bakkali, J.M. Gonzalez-Leal, J.J. Delgado, M. Ramírez-del-Solar, Tracking the optical constants of porous vanadium dioxide thin films during metal–insulator transition: Influence of processing conditions on their application in smart glasses, Appl. Surf. Sci. 580 (2022) 152228. doi:10.1016/j.apsusc.2021.152228.

[24] Y.-B. Kang, Critical evaluation and thermodynamic optimization of the VO–$VO_{2.5}$ system, J. Eur. Ceram. Soc. 32 (2012) 3187–3198. doi:10.1007/s11663-020-01939-0.

[25] P. Shvets, O. Dikaya, K. Maksimova, A. Goikhman, A review of Raman spectroscopy of vanadium oxides, J. Raman Spectrosc. 50 (2019) 1226–1244. doi:10.1002/jrs.5616.

[26] M.G. Krishna, A.K. Bhattacharya, Optical and structural properties of bias sputtered vanadium pentoxide thin films, Vacuum. 48 (1997) 879–882. doi:10.1016/s0042-207x(97)00123-1.

[27] G. Sun, X. Cao, S. Long, R. Li, P. Jin, Optical and electrical performance of thermochromic V_2O_3 thin film fabricated by magnetron sputtering, Appl. Phys. Lett. 111 (2017) 053901. doi:10.1063/1.4997323.

[28] T. Kang, Z. Ma, J. Qin, Z. Peng, W. Yang, T. Huang, S. Xian, S. Xia, W. Yan, Y. Yang, Z. Sheng, J. Shen, C. Li, L. Deng, L. Bi, Large-scale, power-efficient Au/VO_2 active metasurfaces for ultrafast optical modulation, Nanophotonics. 10 (2020) 909–918. doi:10.1515/nanoph-2020-0354.

[29] L. Miao, R. Chen, J. Zhou, C. Liu, Y. Peng, J. Gao, L. Sun, S. Tanemura, Depressed haze and enhanced solar modulation capability for VO_2-based composite films with distinct size effects, RSC Adv. 6 (2016) 90813–90823. doi:10.1039/c6ra16667a.

[30] S. Choi, J. Kang, S. Ryu, H. Jeen, J. Son, S. Lee, High infrared transparency up to 8-μm-wavelength in correlated vanadium Wadsley conductors, APL Mater. 8 (2020) 041111. doi:10.1063/1.5136059.

[31] D. Gu, Y. Li, X. Zhou, Y. Xu, Facile fabrication of composite vanadium oxide thin films with enhanced thermochromic properties, ACS Appl. Mater. Interfaces. 11 (2019) 37617–37625. doi:10.1021/acsami.9b11376.

[32] B. Allabergenov, S. Yun, H.S. Cho, H.K. Lyu, B. Choi, Control of polymorphic properties of multivalent vanadium oxide thin films, ACS Appl. Electron. Mater. 3 (2021) 1142–1150. doi:10.1021/acsaelm.0c01010.

[33] Y. Gao, H. Luo, Z. Zhang, L. Kang, Z. Chen, J. Du, M. Kanehira, C. Cao, Nanoceramic VO_2 thermochromic smart glass: A review on progress in solution processing, Nano Energy. 1 (2012) 221–246. doi:10.1016/j.nanoen.2011.12.002.

[34] K.L. Gurunatha, S. Sathasivam, J. Li, M. Portnoi, I.P. Parkin, I. Papakonstantinou, Combined effect of temperature induced strain and oxygen vacancy on metal-insulator transition of VO_2 colloidal particles, Adv. Funct. Mater. 30 (2020) 2005311. doi:10.1002/adfm.202005311.

[35] L. Chen, X. Wang, D. Wan, Y. Cui, B. Liu, S. Shi, H. Luo, Y. Gao, Tuning the phase transition temperature, electrical and optical properties of VO_2 by oxygen nonstoichiometry: Insights from first-principles calculations, RSC Adv. 6 (2016) 73070–73082. doi:10.1039/c6ra09449j.

[36] N. Shen, S. Chen, R. Shi, S. Niu, A. Amini, C. Cheng, Phase transition hysteresis of tungsten doped VO_2 synergistically boosts the function of smart windows in ambient conditions, ACS Appl. Electron. Mater. 3 (2021) 3648–3656. doi:10.1021/acsaelm.1c00550.

[37] W. Li, S. Ji, Y. Li, A. Huang, H. Luo, P. Jin, Synthesis of VO_2 nanoparticles by a hydrothermal-assisted homogeneous precipitation approach for thermochromic applications, RSC Adv. 4 (2014) 13026–13033. doi:10.1039/c3ra47666a.

[38] A. Simo, B. Mwakikunga, B.T. Sone, B. Julies, R. Madjoe, M. Maaza, VO_2 nanostructures based chemiresistors for low power energy consumption hydrogen sensing, Int. J. Hydrogen Energy. 39 (2014) 8147–8157. doi:10.1016/j.ijhydene.2014.03.037.

[39] J.W. Byon, M. Bin Kim, M.H. Kim, S.Y. Kim, S.H. Lee, B.C. Lee, J.M. Baik, Electrothermally induced highly responsive and highly selective vanadium oxide hydrogen sensor based on metal-insulator transition, J. Phys. Chem. C. 116 (2012) 226–230. doi:10.1021/jp2080989.

[40] X. Gao, C.M.M. Rosário, H. Hilgenkamp, Multi-level operation in VO_2-based resistive switching devices, AIP Adv. 12 (2022) 015218. doi:10.1063/5.0077160.

[41] G. Liu, S. Wang, A.I.Y. Tok, T.J. White, C. Li, M. Layani, S. Magdassi, M. Li, Y. Long, Self-assembled VO_2 mesh film-based resistance switches with high transparency and abrupt ON/OFF ratio, ACS Omega. 4 (2019) 19635–19640.

doi:10.1021/acsomega.9b02239.

[42] L. Kang, Y. Gao, H. Luo, Z. Chen, J. Du, Z. Zhang, Nanoporous thermochromic VO_2 films with low optical constants, enhanced luminous transmittance and thermochromic properties, ACS Appl. Mater. Interfaces. 3 (2011) 135–138. doi:10.1021/am1011172.

[43] M.K. Dietrich, B.G. Kramm, M. Becker, B.K. Meyer, A. Polity, P.J. Klar, Influence of doping with alkaline earth metals on the optical properties of thermochromic VO_2, J. Appl. Phys. 117 (2015) 185301. doi:10.1063/1.4919433.

[44] D.P. Zhang, M.D. Zhu, Y. Liu, K. Yang, G.X. Liang, Z.H. Zheng, X.M. Cai, P. Fan, High performance VO_2 thin films growth by DC magnetron sputtering at low temperature for smart energy efficient window application, J. Alloys Compd. 659 (2016) 198–202. doi:10.1016/j.jallcom.2015.11.047.

[45] S. Dou, J. Zhao, W. Zhang, H. Zhao, F. Ren, L. Zhang, X. Chen, Y. Zhan, Y. Li, A universal approach to achieve high luminous transmittance and solar modulating ability simultaneously for vanadium dioxide smart coatings via double-sided localized surface plasmon resonances, ACS Appl. Mater. Interfaces. 12 (2020) 7302–7309. doi:10.1021/acsami.9b17923.

[46] S. Liu, C.Y. Tso, H.H. Lee, Y. Zhang, K.M. Yu, C.Y.H. Chao, Bio-inspired TiO_2 nano-cone antireflection layer for the optical performance improvement of VO_2 thermochromic smart windows, Sci. Rep. 10 (2020) 11376. doi:10.1038/s41598-020-68411-6.